Analysis of Collective and Enhanced Individual Pitch Control Strategies for Wind Turbines

Manuel Lara
Department of Electrical Engineering and Automation
University of Cordoba
Cordoba, Spain
0000-0002-0330-2982

Mario L. Ruz
Department of Mechanics, Area of Mechanics
University of Cordoba
Cordoba, Spain
0000-0002-2356-5253

Francisco Vázquez
Department of Electrical Engineering and Automation
University of Cordoba
Cordoba, Spain
0000-0003-4544-6084

Sebastiaan Paul Mulders
Delft Center for Systems and Control
Delft University of Technology
Delft, The Netherlands
0000-0003-4689-257X

Jan-Willem van Wingerden
Delft Center for Systems and Control
Delft University of Technology
Delft, The Netherlands
0000-0003-3061-7442

Juan Garrido
Department of Electrical Engineering and Automation
University of Cordoba
Cordoba, Spain
0000-0001-5122-4803

2026 IEEE 23rd Mediterranean Electrotechnical Conference (MELECON) | 979-8-3315-2684-9/26/$31.00 ©2026 IEEE | DOI: 10.1109/MELECON64486.2026.11418863

Abstract—**In the nominal operating region of wind turbines, collective pitch control (CPC) regulates power by maintaining rated rotor speed, while individual pitch control (IPC) mitigates cyclic blade loads caused by wind variations like wind shear or turbulence. However, tuning CPC presents a significant trade-off, as improving power regulation often leads to an increase in fatigue blade loads. Additionally, IPC implementation via Multi-Blade Coordinate (MBC) transformation suffers from coupling between IPC loops, reducing controller effectiveness. Prior studies suggest that azimuth offset and static inverted decoupling enhance classical IPC implementations by mitigating this coupling. However, a comparative performance analysis between both implementations remains unexplored. This study addresses this analysis through a multi-objective optimization approach to tune CPC and IPC strategies for a 15 MW reference wind turbine. Four configurations (baseline CPC with conventional IPC, CPC+IPC, CPC+IPC with azimuth offset, and CPC+IPC with static inverted decoupling) are optimized. Results show that a well-tuned CPC improves IPC effectiveness, while the incorporation of azimuth offset or static inverted decoupling in IPC significantly improves both objectives, achieving reductions of approximately 19% in damage equivalent load on the blades and 60% in the integral squared error of power output compared to the baseline CPC with conventional IPC, and around 9% and 30% relative to the CPC with conventional IPC.**

Keywords— ***wind turbine control, multi-objective optimization, load mitigation, individual pitch control***

I. INTRODUCTION

Wind energy has become a key renewable source for reducing greenhouse gas emissions and supporting the global energy transition [1]. However, the increasing size of wind turbines introduces significant mechanical loads, impacting structural integrity and maintenance costs. These loads grow non-linearly with turbine size, requiring advanced controllers to mitigate structural stress and extend operational life [2].

Wind turbines operate in different regions based on wind speed [3]. In the nominal region, where wind speed exceeds the rated value, power regulation and load mitigation are managed through blade pitch control. Two primary strategies are employed: collective pitch control (CPC) and individual pitch control (IPC) [4]. CPC uniformly adjusts the pitch angle of all blades to regulate rotor speed and power output [5]. Conversely, IPC adjusts each blade's pitch individually to counteract asymmetric loads caused by wind shear, turbulence, and yaw misalignment. By reducing cyclic loads, IPC minimizes structural fatigue, improving turbine reliability and extending lifespan [6]. Fig. 1 shows the control scheme integrating CPC and IPC. Individual pitch signals are superimposed onto the collective pitch signal to determine the final pitch angle for each blade. Operating in the full-load region at rated power, the wind turbine maintains a constant generator torque T_g, at its nominal value.

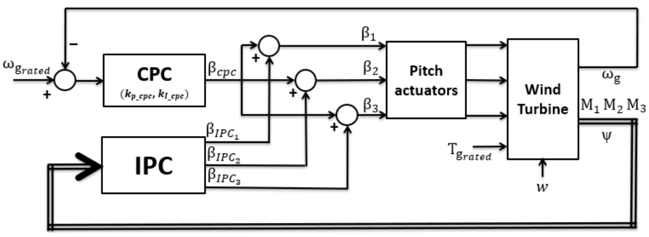

Fig. 1. IPC+CPC control system scheme for the full load region.

While CPC is primarily designed for power regulation, its tuning affects aerodynamic loads on the blades. A poorly tuned CPC can induce oscillations, increasing cyclic loads and structural fatigue. In turbulent wind conditions, an inadequate CPC may fail to respond effectively, leading to higher stress on turbine components. IPC, on the other hand, directly mitigates asymmetric loads but requires careful tuning to avoid interference with CPC. Studies have shown that IPC can significantly reduce equivalent damage loads (DEL) without affecting energy production [7]. However, its effectiveness depends on proper coordination with CPC. Focusing solely on IPC for fatigue reduction may decrease energy efficiency, while prioritizing CPC for power regulation can increase structural loads and accelerate component wear.

Another challenge in IPC implementation arises from the Multi-Blade Coordinate (MBC) transformation, which converts blade loads from the rotating frame to a fixed frame, representing them as tilt and yaw moments. This transformation facilitates IPC design for fatigue load mitigation at specific frequencies, such as 1P harmonics. However, research indicates that MBC transformation does not completely decouple tilt and yaw axes due to blade dynamics, actuator phase loss, control system time delays, and aerodynamic interactions [8], [9]. This residual coupling

This research was funded by the Spanish Ministry of Science, Innovation and Universities under granted project PID2023-149181OB-I00 (MCIU/AEI/10.13039/501100011033/FEDER, UE).

introduces cross-effects that reduce the effectiveness of conventional single-input single-output (SISO) controllers, potentially amplifying undesired loads.

To address these issues, recent studies have explored advanced IPC strategies, such as azimuth offset and static inverted decoupling. Azimuth offset minimizes tilt-yaw interactions, improving IPC effectiveness [10]. Static inverted decoupling, on the other hand, uses a decoupling network to reduce inter-axis dependencies, enhancing controller independence [11]. Although both techniques have shown promise [11], [12], a direct comparison of their performance remains unexplored. This study aims to analyze the impact of CPC and IPC strategies on energy production and fatigue blade loads in large-scale wind turbines. The main contributions of this paper are:

- A proposal of a multi-objective optimization framework based on Pareto front analysis with genetic algorithm. This framework simultaneously tunes CPC and IPC strategies to achieve a balanced trade-off between blade fatigue load reduction and power regulation in the IEA 15 MW reference wind turbine.
- A comparative analysis of advanced IPC strategies, incorporating azimuth offset and static inverted decoupling to mitigate tilt-yaw coupling in the MBC transformation. This demonstrates the superior effectiveness of these control schemes over conventional IPC approaches.
- Analysis of control parameter interdependencies to guide the coordinated design of CPC and IPC.

This paper is structured as follows: Section 2 provides background information on IPC implementation and static inverted decoupling. Section 3 details the optimization methodology and parameter tuning procedure. Section 4 presents the comparative analysis of the proposed controllers and the baseline configuration. Finally, Section 5 summarizes the conclusions and future research directions.

II. Background

A. Individual Pitch Control

The most common implementation of IPC involves the use of the MBC transformation, which converts the blade load measurements from a rotating frame into a fixed (non-rotating) reference frame. In this fixed frame, the loads are typically represented as two components: the tilt moment (M_t) and the yaw moment (M_y). These moments are then used as inputs to a feedback control system, which generates pitch commands to reduce these loads. The MBC transformation is defined as:

$$\begin{bmatrix} M_{\mathrm{t}}(t) \\ M_{\mathrm{y}}(t) \end{bmatrix} = \boldsymbol{T}(\boldsymbol{\psi})\, \boldsymbol{M}(t), \tag{1}$$

where $\boldsymbol{T(\psi)}$ is the forward MBC transformation matrix, and $M(t)$ is the vector of out-of-plane (OoP) bending moments measured at the blade roots. The matrix $\boldsymbol{T(\psi)}$ is given by:

$$\boldsymbol{T}(\boldsymbol{\psi}) = \frac{2}{3} \begin{bmatrix} \cos(\psi_1) & \cos(\psi_2) & \cos(\psi_3) \\ \sin(\psi_1) & \sin(\psi_2) & \sin(\psi_3) \end{bmatrix}, \tag{2}$$

where ψ_i represents the azimuth angle of the i-th blade, and the number of blades is three.

Once the fixed-frame moments are computed, a decentralized control system is used to generate the pitch commands for the tilt and yaw axes. These commands are then transformed back into the rotating frame using the inverse MBC transformation, resulting in individual pitch angles for each blade. The inverse transformation is given by:

$$\begin{bmatrix} \beta_{IPC1}(t) \\ \beta_{IPC2}(t) \\ \beta_{IPC3}(t) \end{bmatrix} = \boldsymbol{T}^{-1}(\boldsymbol{\psi} + \psi_o) \begin{bmatrix} \beta_t(t) \\ \beta_y(t) \end{bmatrix}, \tag{3}$$

where $\beta_t(t)$ and $\beta_y(t)$ are the pitch commands in the fixed frame, and ψ_o is the azimuth offset. This offset is an additional tuning parameter that can be introduced to improve the decoupling between the tilt and yaw axes [10]. The computation of this transformation is achieved through the reverse MBC transformation in (4).

$$\boldsymbol{T}^{-\mathbf{1}}(\boldsymbol{\psi} + \psi_o) = \begin{bmatrix} \cos(\psi_1 + \psi_o) & \sin(\psi_1 + \psi_o) \\ \cos(\psi_2 + \psi_o) & \sin(\psi_2 + \psi_o) \\ \cos(\psi_3 + \psi_o) & \sin(\psi_3 + \psi_o) \end{bmatrix} \tag{4}$$

B. Static inverted decoupling

Static inverted decoupling is an multivariable control technique designed to mitigate interactions between system variables, allowing control loops to operate more independently [13] (Fig. 2). In conventional decoupling methods, control signals are generated through a weighted combination of outputs from decentralized controllers. However, inverted decoupling proposes an alternative structure in which each control signal is derived from the output of a primary controller combined with other system control signals. This approach aims to maintain apparent processes similar to the diagonal ones of the original system, using simpler decoupling elements that facilitate practical design and implementation [13].

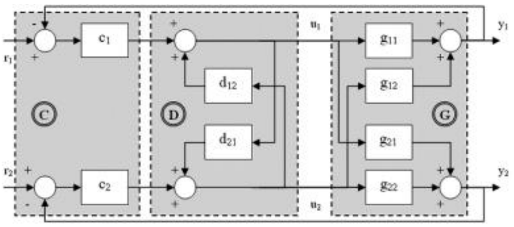

Fig. 2. Inverted decoupling [13].

$$\begin{pmatrix} M_{\mathrm{t}}(s) \\ M_{\mathrm{y}}(s) \end{pmatrix} = \boldsymbol{G}(s) \begin{pmatrix} \beta_{\mathrm{t}}(s) \\ \beta_{\mathrm{t}}(s) \end{pmatrix} = \begin{pmatrix} g_{11}(s) & g_{12}(s) \\ g_{21}(s) & g_{22}(s) \end{pmatrix} \begin{pmatrix} \beta_{\mathrm{t}}(s) \\ \beta_{\mathrm{y}}(s) \end{pmatrix} \tag{5}$$

The principle of inverted decoupling is illustrated for a 2×2 system, where the process model is represented by a transfer function matrix $\boldsymbol{G(s)}$ as shown in equation (5). When applied to the IPC framework, $g_{ij}(s)$ is the transfer function between the i-th output and the j-th control signal. In this case, the controlled variables are the tilt and yaw moments, and the control signals are the tilt and yaw pitch signals [11].

$$\boldsymbol{D}(s) = \boldsymbol{G}^{-\mathbf{1}}(s) \begin{pmatrix} g_{11}(s) & 0 \\ 0 & g_{22}(s) \end{pmatrix} = \tag{6}$$

$$= \frac{\begin{pmatrix} g_{11}(s)g_{22}(s) & -g_{12}(s)g_{22}(s) \\ -g_{21}(s)g_{11}(s) & g_{11}(s)g_{22}(s) \end{pmatrix}}{g_{11}(s)g_{22}(s) - g_{12}(s)g_{21}(s)}$$

In a conventional decoupling network, ideal decoupling is the equivalent to inverted decoupling. However, this design can be challenging to implement in practice due to the complexity of the elements in $D(s)$, as shown in (6). Inverted decoupling offers an alternative that achieves a diagonal apparent process with simpler elements in (7) [13]. Thus, the decoupling matrix becomes that shown in (8).

$$d_{12}(s) = \frac{-g_{12}(s)}{g_{11}(s)} \text{ and } d_{21}(s) = \frac{-g_{21}(s)}{g_{22}(s)}. \tag{7}$$

$$\mathbf{D}(s) = \frac{\begin{pmatrix} 1 & d_{12}(s) \\ d_{21}(s) & 1 \end{pmatrix}}{1-d_{12}(s)d_{21}(s)} \tag{8}$$

Static inverted decoupling relies on the steady-state gain matrix *G(0)*. This approach is particularly useful in applications with slow dynamics, where interactions can be mitigated through steady-state adjustments. The static decoupling elements are derived directly from *G(0)* at *s=0*, further simplifying the design and implementation compared to dynamic inverted decoupling [13]. These gains ensure that the apparent process is diagonal at steady state with $g_{11}(0)$ and $g_{22}(0)$, reducing interactions at low frequencies. Dynamic decoupling elements may be necessary when process interactions are more relevant at medium frequencies.

$$d_{12}(0) = -\frac{g_{12}(0)}{g_{11}(0)} \quad d_{21}(0) = -\frac{g_{21}(0)}{g_{22}(0)} \tag{9}$$

III. Proposed Methodology

This study presents a co-simulation framework for a wind turbine model, using OpenFAST in MATLAB/Simulink. The simulations are based on the IEA 15 MW reference wind turbine, configured as an offshore monopile structure, with its key design parameters outlined in [14]. For the purposes of this work, the turbine is analyzed exclusively within the full-load region, where high wind speeds induce significant blade loading due to amplified bending moments [15].

To replicate realistic wind conditions, turbulent inflow fields were generated using TurbSim. The selected operating condition corresponds to a mean wind speed of 22 m/s. The wind profiles adhere to the IEC standard [16]. They employ a Kaimal turbulence model, characterized by a hub-height turbulence intensity of 10% and a vertical wind shear described by a power-law exponent of 0.2. The simulations were conducted with a sampling frequency of 200 Hz to capture the dynamic response of the system accurately.

A. CPC and IPC schemes

The CPC efficiently counteracts wind speed variations to maintain the rotor speed at its rated value, ensuring the generated power remains at its nominal value ($P_{g,rated}$). The CPC employs a Proportional-Integral (PI) controller with proportional gain (k_{p_cpc}) and integral gain (k_{i_cpc}). As illustrated in Fig. 3, the IPC scheme incorporates the MBC transformation to address the 1P harmonic; then, it uses internal control to reduce tilt (M_t) and yaw (M_y) moments, followed by a reverse MBC transformation that optionally includes an azimuth offset (ψ_o). The internal control comprises two integral controllers (with gains k_{I_tilt} and k_{I_yaw}), with the option to incorporate static inverted decoupling gains (d_{12} and d_{21}) as previously described. Using azimuth offset or static inverted decoupling enhances the decoupling of tilt and yaw axes. This can potentially achieve greater reductions in periodic blade loads than an IPC configuration with neither offset (ψ_o= 0º) nor decoupling (d_{12}=d_{21}=0).

This study investigates the trade-off between power regulation and blade load reduction in CPC while mitigating tilt-yaw interactions in IPC. The study proposes four CPC-IPC configurations that progressively incorporate advanced control techniques. These configurations, based on the parameters described above, are:

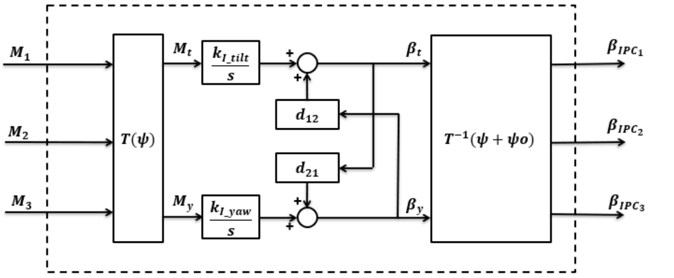

Fig. 3. 1P IPC scheme with option of static inverted decoupling or azimuth offset.

- ROSCO-IPC (ψ_o= 0º, d_{12}=d_{21}=0): utilizes a pre-tuned gain-scheduled PI-based CPC from the open-source ROSCO controller [17], paired with IPC employing two identical integral controllers ($k_{I\_tilt} = k_{I\_yaw}$) with no decoupling. The only optimized parameter is the common IPC integral gain k_{i_IPC}= k_{I_tilt} =k_{I_yaw}. It serves as a baseline.

- CPC-IPC (ψ_o= 0º, d_{12}=d_{21}=0): introduces a custom PI-based CPC, enabling coordinated tuning of CPC and IPC parameters to better balance the conflicting objectives. It has three parameters to be optimized: two CPC parameters (k_{p_cpc} and k_{i_cpc}) and the same IPC gain (k_{i_IPC}).

- CPC-IPC-Azi (ψ_o≠0º, d_{12}=d_{21}=0): extends CPC-IPC with an azimuth offset, optimizing four parameters (k_{p_cpc}, k_{i_cpc}, k_{i_IPC}, ψ_o).

- CPC-IPC-D (ψ_o=0º, d_{12}≠0, d_{21}≠0): extends the CPC-IPC configuration by incorporating static inverted decoupling. Following a prior analysis of the 2×2 process for IPC, and to align the number of parameters with the CPC-IPC-Azi scheme, two decoupling elements are used that are identical in absolute value but opposite in sign (d_o= d_{12}=-d_{21}). Four parameters are optimized (k_{p_cpc} , k_{i_cpc}, k_{i_IPC}, d_o).

B. CPC-IPC tuning procedure by optimization

This section outlines the multi-objective optimization (MOO) framework developed to determine the optimal parameter settings for the CPC and IPC systems. To address the inherent trade-off between blade fatigue reduction and power output regulation, this study formulates the CPC-IPC tuning as a MOO problem. The optimization targets two key objectives encapsulated in the cost function vector *J*= [DEL(*M*) ISE(P_g)]. The first objective, DEL(*M*), quantifies the damage equivalent load (DEL) associated with the OoP moments of the blades, aiming to minimize fatigue. The DEL is a widely adopted metric in wind turbine fatigue analysis, typically computed offline from simulation time series using cycle-counting methods. Real-time analytical DEL computation is impractical. This work employs the MLife script suite [18] to post-process simulation data from each run, extracting the mean DEL across the three blade OoP moments, denoted as DEL(*M*), as the fatigue-related cost function.

The second objective, ISE(P_g), measures the integral of the squared error between the turbine's rated power, $P_{g,rated}$, and the actual generated power, P_g, as shown in (10). This metric reflects the CPC's effectiveness in maintaining consistent generator speed and power output, serving as the performance index for power regulation.

$$\mathrm{ISE}(P_g) = \int \left(P_{g,rated} - P_g(t)\right)^2 dt \qquad (10)$$

Four CPC-IPC configurations are optimized and compared. The parameter vector $\rho = [k_{p\_cpc}, k_{i\_cpc}, k_{i\_IPC}, d_o, \psi_o]$ varies depending on the configuration, with specific components enabled or disabled based on the control scheme. Solving this MOO problem follows the workflow depicted in Fig. 4. The approach leverages Pareto fronts to explore trade-offs and employs decision-making tools to select the most suitable solution. Due to the complexity of the objective functions in J and the nonlinear dynamics of the wind turbine model, analytical solutions are infeasible. Instead, a simulation-driven optimization strategy is adopted, to evaluate the cost function across numerous co-simulations.

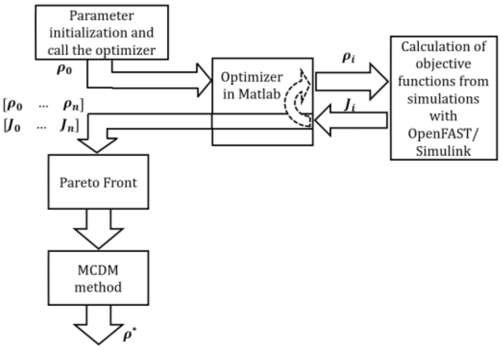

Fig. 4. Flowchart illustrating the multi-objective optimization procedure for tuning CPC and IPC parameters.

The optimization process begins by initializing the decision variables in ρ_0. An iterative loop then employs a MATLAB-based optimizer to conduct simulations, compute J, and map the Pareto front. This nonlinear optimization task demands significant computational effort. To enhance efficiency, the nondominated sorting genetic algorithm-II (NSGA-II) is utilized [19]. NSGA-II, an evolutionary algorithm tailored for MOO, excels at navigating multi-objective solution spaces. The resulting Pareto front solutions are evaluated using multi-criteria decision-making (MCDM) techniques to identify the preferred configuration based on specific priorities. Among these, the Technique for Order of Preference by Similarity to Ideal Solution (TOPSIS) is selected due to its widespread use in energy-related optimization studies [20]. TOPSIS ranks solutions by their proximity to an ideal point, yielding the final optimal parameter set. Search ranges for the parameters are detailed in Table I. Population sizes are tailored to each scheme: 1600 individuals (8×8×5×5) for configurations with four parameters, 320 (8×8×5) for those with three, and 100 for single-parameter cases. Other genetic algorithm settings include a maximum of 60 generations and a Pareto front population of 25 individuals. This MOO approach ensures a robust and fair comparison of the CPC-IPC schemes.

IV. Results

A. Multi-objective optimization results

This section presents the results of the MOO of the proposed CPC-IPC schemes, evaluated through 400-s simulations with a turbulent wind profile at a mean speed of 22 m/s. Fig. 5 displays the Pareto fronts for the four configurations illustrating the trade-off between DEL(M) and ISE(P_g). Optimal solutions, selected via the TOPSIS method, are marked with stars: blue for ROSCO-IPC, red for CPC-IPC, black for CPC-IPC-Azi, and green for CPC-IPC-D. The ROSCO-IPC scheme exhibits an insignificant Pareto front, indicating limited trade-off flexibility due to its reliance on a single parameter (k_{i_IPC}), with improvements in ISE(P_g) minimally affecting DEL(M). Tuning the CPC parameters (k_{p_cpc}, k_{i_cpc}) in the CPC-IPC scheme shifts the Pareto front leftward, extending it toward lower DEL values. This confirms that tuning the CPC enhances load compensation without sacrificing the quality of power tracking. This improvement is further enhanced in CPC-IPC-Azi and CPC-IPC-D, where the inclusion of ψ_o and d_o allows for displacing the fronts further left with DEL(M) minimal. Both configurations outperform ROSCO-IPC and CPC-IPC.

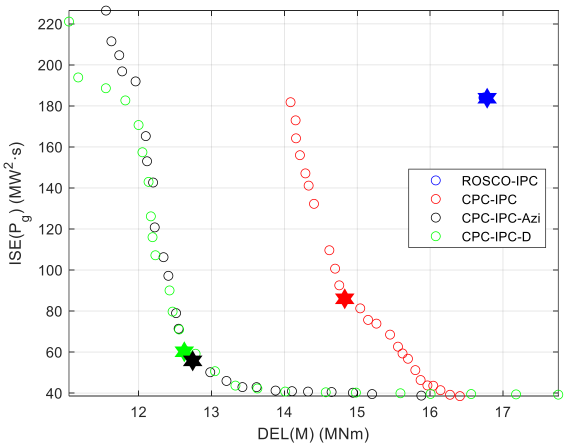

Fig. 5. Pareto fronts (ISE(P_g) vs DEL(M)) for the differents CPC+IPC.

Fig. 6 explores the relationships between control parameters and objectives. In CPC-IPC, CPC-IPC-Azi, and CPC-IPC-D, more negative $k_{p,cpc}$ values correlate with higher DEL(M) but lower ISE(P_g). This indicates that less aggressive proportional control reduces loads at the expense of power regulation. Conversely, more negative k_{i_cpc} values reduce ISE(P_g) but increase DEL(M) highlighting the trade-off between power regulation and load reduction. The k_{i_IPC} subplot reveals that higher values reduce DEL(M) up to a threshold, beyond which ISE(P_g) increases due to IPC-induced oscillations. Interdependencies show that more negative $k_{p,cpc}$ and $k_{i,cpc}$ values are paired, and they support higher k_{i_IPC}, while ψ_o and d_o expand range of k_{i_IPC}, enhancing load reduction. These interdependencies underscore the need for coordinated tuning of CPC and IPC.

TABLE I. Optimal CPC-IPC parameters and objective values for the optimization wind condition

Controller	$k_{p,cpc}$ (deg/rpm)	$k_{i,cpc}$ (deg·s/rpm)	k_{i_IPC} (rad·kNm^{-1}s^{-1})	d_o (-)	ψ_o (º)
Search ranges	[-1 to 0]	[-0.1 to 0]	[0 to $5\cdot10^{-5}$]	[0-10]	[0-90]
ROSCO-IPC	-	-	$7.37\cdot10^{-8}$	-	-
CPC-IPC	-0.3556	-0.0029	$2.25\cdot10^{-7}$	-	-
CPC-IPC-Azi	-0.4203	-0.0232	$1.77\cdot10^{-6}$	-	72.9
CPC-IPC-D	-0.3801	-0.0229	$6.33\cdot10^{-6}$	3.39	-

B. Simulation results

This section evaluates in greater detail the performance of the optimized CPC-IPC schemes with the optimal parameters in Table I. For this purpose, six 1000-s simulation cases were conducted, using different wind profiles with a mean wind speed of 22 m/s and identical turbulent properties as those employed during the optimization phase. These simulations enable a robust assessment of each control scheme's performance under variable yet comparable wind conditions, adhering to the IEC standard.

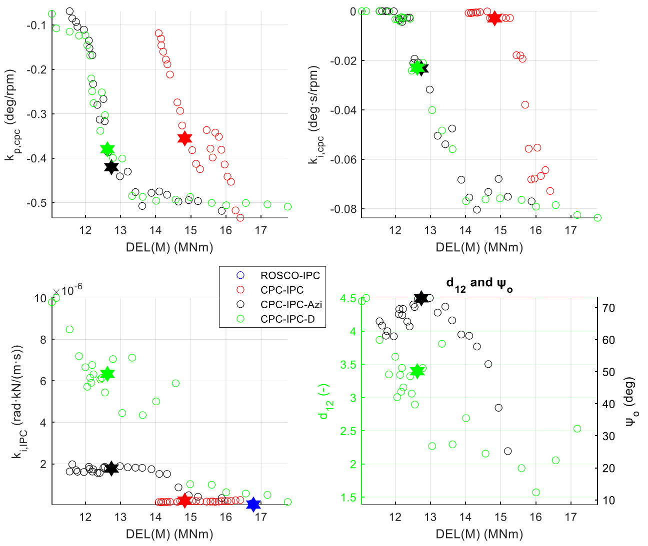

Fig. 6. Relationships between control parameters and DEL(M) for the different CPC-IPC configurations.

Fig. 7 shows a bar chart with the values of DEL(M) (in MN·m) and ISE(P_g) (in MW²·s) for the proposed CPC-IPC schemes across the six simulation cases. Similar DEL(M) and ISE(P_g) values were obtained for each controller across the different simulations, with minor variations attributable to the stochastic nature of the turbulent wind profiles. Notably, the ISE(P_g) values obtained during the optimization process (conducted over 400 seconds) were lower than those recorded in the 1000-s validation simulations. This discrepancy arises because ISE(P_g) grows linearly with time if the error maintains a constant or statistically similar behavior, as is the case with the employed wind profiles. In contrast, DEL(M) provides a reliable metric for fatigue damage load in a standardized format, regardless of simulation duration.

Analyzing the results by controller and seed, ROSCO-IPC consistently exhibits the highest fatigue loads and power fluctuations across all wind profiles, indicating limited effectiveness in mitigating structural demands and power output regulation. In contrast, the optimized CPC-IPC scheme achieves noticeable reductions in both objectives, reflecting the benefits of coordinated pitch control tuning. The advanced configurations, CPC-IPC-Azi and CPC-IPC-D, demonstrate even greater improvements. These schemes consistently outperform the baseline and basic CPC-IPC by achieving lower fatigue loads and enhanced power regulation, highlighting the advantages of minimizing tilt-yaw interactions. Both advanced schemes show comparable performance.

Table II presents the average values of DEL(M), ISE(P_g), and NAT(β) across the six 1000-s simulations for the proposed optimal CPC-IPC schemes. The NAT(β), which measures control effort through the normalized actuator travel of the pitch actuators, remains stable, ranging from 50% (ROSCO-IPC) to 52.1% (CPC- IPC-Azi). This suggests that the improvements in load and power performance do not significantly increase control effort. The NAT(β) is defined as:

$$NAT(\beta) = \frac{1}{3}\sum_{i=1}^{3}\left(\frac{1}{T}\int_0^T \left|\frac{\dot{\beta}_i(t)}{\dot{\beta}_{\max}}\right| dt\right). \tag{11}$$

Table II also highlights the relative performance, expressed as percentages relative to baseline ROSCO-IPC, underscoring the advantages of the proposed schemes. The CPC-IPC achieves a DEL(M) reduction to 91.8% and an ISE(P_g) reduction to 57.6%, demonstrating a balance between fatigue load reduction and power regulation. The CPC-IPC-Azi, incorporating an optimal azimuthal offset, reduces DEL(M) to 81.5% and ISE(P_g) to 37.6%, highlighting the benefit of decoupling the tilt and yaw axes. Similarly, the CPC-IPC-D, with static inverse decoupling, achieves 80.9% for DEL(M) and 40.4% for ISE(P_g), aligning with the performance of CPC-IPC-Azi. Compared to ROSCO-IPC, which uses a predefined controller without CPC adjustments, the CPC-IPC, CPC-IPC-Azi, and CPC-IPC-D schemes offer significant improvements.

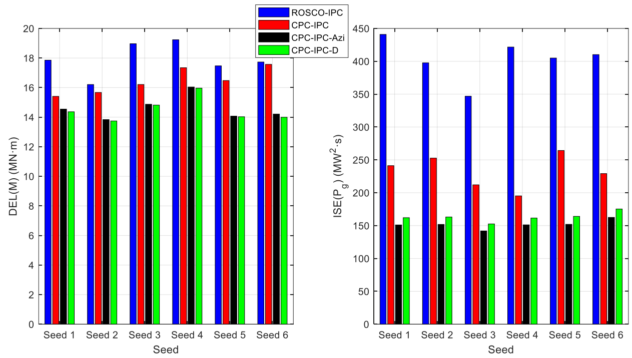

Fig. 7. Bar Chart of DEL(M) and ISE(P_g) for Different Seeds

TABLE II. AVERAGE PERFORMANCE METRICS FOR OPTIMIZED CPC-IPC SCHEMES

Controller	$\overline{\mathbf{DEL}}(\boldsymbol{M})$ (MN·m)	$\overline{\mathbf{ISE}}(P_g)$ (MW²·s)	$\overline{\mathbf{NAT}}(\boldsymbol{\beta})$ (%)
ROSCO- IPC	17.9 (100%)	403.7 (100%)	50.0
CPC-IPC	16.4 (91.8%)	232.4 (57.6%)	51.9
CPC-IPC-Azi	14.6 (81.5%)	151.8 (37.6%)	52.1
CPC-IPC-D	14.5 (80.9%)	163.1 (40.4%)	52.0

Fig. 8 presents a example of the time-domain response of the different control strategies over an 800–900 second interval from one of the six evaluated seeds. This interval allows for a qualitative comparison of the power generated (P_g), the OoP bending moment for blade 1 (M_1), and the pitch angle for blade 1 (β_1) under turbulent wind conditions with speeds varying between 20.7 m/s and 26.7 m/s. CPC-IPC-D and CPC-IPC-Azi show the best P_g regulation, with amplitudes 37–38.7% lower than ROSCO-IPC, enhancing the quality of the generated power. In terms of M_1, these configurations reduce the amplitude of loads by 36%. The larger β_1 range in CPC-IPC-D and CPC-IPC-Azi indicates a more active control effort, required by these benefits, consistent with the NAT(β) increase of 2.1% observed in Table II. Conversely, ROSCO-IPC exhibits greater oscillations in P_g and M_1, reflecting its limited load mitigation capability, while CPC-IPC offers an intermediate performance with a more stable β_1 range but less load reduction.

V. CONCLUSIONS

This study demonstrates the efficacy of a MOO framework for tuning CPC and IPC strategies, achieving an effective balance between power regulation and blade load mitigation in the IEA 15 MW reference wind turbine. Proper coordination between these control systems is critical: a poorly tuned CPC can induce oscillations that compromise power stability and regulation, while an overly aggressive IPC may reduce energy efficiency.

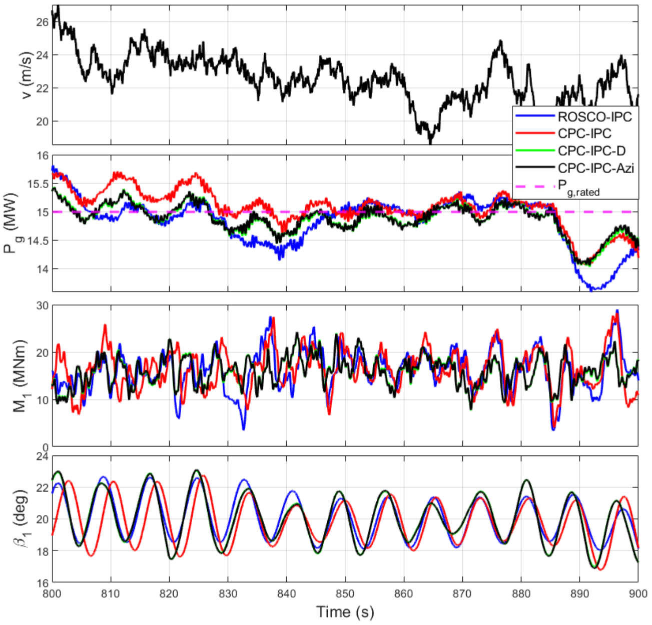

Fig. 8. Time-domain response of CPC-IPC strategies (800–900 s)

The results highlight that CPC tuning, beyond its conventional role in power regulation, significantly reduces structural loads by stabilizing rotor dynamics, thereby enhancing IPC effectiveness. Advanced IPC schemes, such as those incorporating azimuth offset or static inverted decoupling, outperform conventional configurations. They reduces the DEL(M) around to 81% and the integral squared error of power ISE(P_g) around to 39% relative to the ROSCO-IPC baseline. Notably, both azimuth offset and static inverted decoupling exhibit similar performance, suggesting that they are equally effective strategies for improving turbine operation. Analysis of the control parameters reveals distinct patterns in their impact. A strong negative correlation between DEL(M) and ISE(P_g) underscores the inherent trade-off across all configurations, which has been successfully managed using the TOPSIS method as a MCDM tool.

The proposed methodology can be extended to other operating points with different mean wind speeds or turbulence intensities. The different sets of tuning parameters can be integrated via a gain-scheduled approach for industrial implementation. It can also be applied to fixed-bottom wind turbines of different sizes. However, its main disadvantage is that it cannot be performed online due to its high computational cost to run the optimization. The computational time is in the order of tens of hours, which is in line with that of other works based on a simulation approach using OpenFAST. To further extend the impact of this work, extrapolating these strategies to floating wind turbines presents a promising opportunity, given the growing interest in this technology and the unique dynamic challenges it poses.

REFERENCES

[1] H. M. Hassan, A. L. ElShafei, W. A. Farag, and M. S. Saad, "A robust LMI-based pitch controller for large wind turbines," Renew Energy, vol. 44, pp. 63–71, 2012, doi: 10.1016/j.renene.2011.12.016.

[2] A. Grapentin, C. A. Hans, and J. Raisch, "Robust LQ Optimal Control for Wind Turbine Power Tracking Operation," IEEE 63rd Conference on Decision and Control (CDC), Jul. 2024, Accessed: Mar. 18, 2025. [Online]. Available: https://arxiv.org/abs/2407.20922v1

[3] N. J. Abbas, P. Bortolotti, C. Kelley, J. Paquette, L. Pao, and N. Johnson, "Aero-servo-elastic co-optimization of large wind turbine blades with distributed aerodynamic control devices," Wind Energy, vol. 26, no. 8, pp. 763–785, Aug. 2023, doi: 10.1002/WE.2840.

[4] A. El Yaakoubi, A. Bouzem, R. El Alami, N. Chaibi, and O. Bendaou, "Wind turbines dynamics loads alleviation: Overview of the active controls and the corresponding strategies," Ocean Engineering, vol. 278, p. 114070, 2023.

[5] Q. Wang, Z. Du, W. Chen, J. Zhang, Y. Lin, and H. Liu, "Incremental feedforward collective pitch control method for wind turbines," Front Energy Res, vol. 11, p. 1326248, Dec. 2023, doi: 10.3389/FENRG.2023.1326248/BIBTEX.

[6] E. A. Bossanyi, "Individual Blade Pitch Control for Load Reduction," Wind Energy, vol. 6, no. 2, pp. 119–128, Apr. 2003, doi: 10.1002/we.76.

[7] C. Santoni, A. Khosronejad, P. Seiler, and F. Sotiropoulos, "Toward control co-design of utility-scale wind turbines: Collective vs. individual blade pitch control," Energy Reports, vol. 9, pp. 793–806, Dec. 2023, doi: 10.1016/J.EGYR.2022.12.041.

[8] M. Geyler and P. Caselitz, "Robust multivariable pitch control design for load reduction on large wind turbines," Journal of Solar Energy Engineering, Transactions of the ASME, vol. 130, no. 3, pp. 0310141–03101412, Aug. 2008, doi: 10.1115/1.2931510/469296.

[9] A. Routray, N. Sivakumar, S. H. Hur, and D. J. Bang, "A Comparative Study of Optimal Individual Pitch Control Methods," Sustainability 2023, Vol. 15, Page 10933, vol. 15, no. 14, p. 10933, Jul. 2023, doi: 10.3390/SU151410933.

[10] S. P. Mulders, A. K. Pamososuryo, G. E. Disario, and J.-W. van Wingerden, "Analysis and optimal individual pitch control decoupling by inclusion of an azimuth offset in the multiblade coordinate transformation," Wind Energy, vol. 22, no. 3, pp. 341–359, Mar. 2019, doi: 10.1002/we.2289.

[11] M. Lara, F. Vázquez, and J. Garrido, "Decentralized Individual Pitch Control with Inverted Decoupling for Wind Turbines in the Full Load Region," in 2024 IEEE 19th Conference on Industrial Electronics and Applications (ICIEA), 2024, pp. 1–6.

[12] M. Lara, S. P. Mulders, J.-W. van Wingerden, F. Vázquez, and J. Garrido, "Analysis of Adaptive Individual Pitch Control Schemes for Blade Fatigue Load Reduction on a 15 MW Wind Turbine," Applied Sciences, vol. 14, no. 1, p. 183, Dec. 2023, doi: 10.3390/app14010183.

[13] J. Garrido, F. Vázquez, F. Morilla, and T. Hägglund, "Practical advantages of inverted decoupling," Proceedings of the Institution of Mechanical Engineers, Part I: Journal of Systems and Control Engineering, vol. 225, no. 7, pp. 977–992, Nov. 2011, doi: 10.1177/2041304110394556.

[14] E. Gaertner et al., "Definition of the IEA Wind 15-Megawatt Offshore Reference Wind Turbine Technical Report," Technical Report NREL/TP-5000-75698, 2020.

[15] A. Natarajan, "Damage equivalent load synthesis and stochastic extrapolation for fatigue life validation," Wind Energy Science, vol. 7, no. 3, pp. 1171–1181, Jun. 2022, doi: 10.5194/wes-7-1171-2022.

[16] IEC 61400–1, "Wind turbines-Part 1: Design requirements," 2005, Accessed: Apr. 24, 2023. [Online]. Available: www.iec.ch/searchpub

[17] NREL, "NREL's Reference OpenSource Controller (ROSCO) toolbox for wind turbine applications.," 2019.

[18] "MLife | Wind Research | NREL." Accessed: Feb. 17, 2025. [Online]. Available: https://www.nrel.gov/wind/nwtc/mlife.html

[19] K. Deb, A. Pratap, S. Agarwal, and T. Meyarivan, "A fast and elitist multiobjective genetic algorithm: NSGA-II," IEEE Transactions on Evolutionary Computation, vol. 6, no. 2, pp. 182–197, Apr. 2002, doi: 10.1109/4235.996017.

[20] V. Bakırcıoğlu, H. B. Jond, and F. Yilmaz, "Multi-Objective optimization and thermodynamic analysis of a supercritical CO2 Brayton cycle in a solar-powered multigeneration plant for net-zero emission goals," Energy Convers Manag, vol. 328, Mar. 2025